Study on Calculation Model of High Speed Machine Silicon Steel Sheet Electromagnetic Characteristics Considering Magnetic, Stress and Temperature Condition

Yu Li, Guangwei Liu, *Member, IEEE*, Wenping Cao, *Senior Member, IEEE*, and Fengge Zhang, *Member, IEEE*

***Abstract*—High-speed motor has the characteristics of high frequency, high temperature, and more stress, resulting in the field distribution inside the motor being complicated. To better study the electromagnetic characteristics of silicon steel sheet for high-speed motor. In this article, a study on the calculation model of silicon sheet electromagnetic characteristics considers the effects of electromagnetic, stress, and temperature factors. The study is divided into two parts, one is to propose the calculation model of silicon steel sheet's permeability; the other is to improve the calculation model of silicon steel sheet's loss. Then, the magnetic field, stress field, and temperature field of a surface mount high speed permanent magnet motor (SMHSPMSM) are analyzed by finite element method (FEM), and the results under the consideration of magnetic, stress, and temperature factors are brought into the calculation model for calculation. Finally, the accuracy of the calculation model for electromagnetic characteristics of silicon steel sheet is verified by comparing the calculated results with the finite element results.**

***Index Terms*—Calculation model, Silicon steel sheet, Electromagnetic characteristics, Magnetic, Stress, Temperature.**

I. INTRODUCTION

NOWADAYS, High-speed permanent magnet motors are widely used in aerospace, machine tools, flywheel energy storage and other fields [1]-[4]. Due to high frequency, high temperature, high power density and other characteristics of the problem has been a hot topic of research [5],[6]. Among them, the research of the rotor core material is also extensive [7],[8], As the main material of motor core, the research of silicon steel sheet is more comprehensive.

Reference [9] has studied that in the production process of silicon steel sheet, the diffusion of residual stress caused by cutting on the whole sample sheet leads to the decline of magnetic conductivity and increase of loss. Some researchers found that water cutting can ensure the magnetic conductivity of silicon steel sheet at low frequency. As the number of shear strips increases, the magnetic conductivity decreases and the loss increases [10]. In order to reduce the impact of blanking and shearing edge effect, the oriented silicon steel sheet is generally annealed to restore its magnetic conductivity and reduce no-load loss [11]. The magnetic conductivity increases with the increase of temperature, and the longer annealing time is more favorable to the recovery of magnetic conductivity at the same annealing temperature. Inert gases can protect annealing from oxidation and nitrification [12].

Research shows that the magnetic conductivity of silicon steel sheet is closely related to magnetic field, stress and temperature [13]-[15]. The higher the frequency of the magnetic field, the worse its permeability, and the larger the area of the hysteresis loop [16]. Reference [17] found that when the magnetization direction is parallel to the rolling direction, the compressive stress along the rolling direction or the tensile stress perpendicular to the direction of the sample will lead to the deterioration of magnetic properties. The increase in temperature causes the permeability to increase first and then decrease [18].

As for the loss of silicon steel sheet, Reference [19] studied the chemical composition of the material and found that with the increase of silicon content, the hysteresis loss of silicon steel sheet decreased significantly. From the perspective of magnetic field, dc bias and non-sinusoidal input signals will lead to increased losses [20],[21]. From the perspective of stress field, the loss of silicon steel sheet increases first and then remains stable at the action of compressive stress [22],[23]. From the perspective of temperature field, the loss of silicon steel sheet can be reduced with the increase of temperature [24]. And based on different influencing factors, several loss-calculation models have been proposed and validated in

Manuscript received December 15, 2021; revised January 31, 2022; accepted March 24, 2022. date of publication September 25, 2022; date of current version September 18, 2022.

This work is by the Key International Cooperation of National Natural Science Foundation of China under Grant 51920105011, Liaoning BaiQianWan Talents Program, and the Natural Science Foundation of LiaoNing Province under Grant 2021-YQ-09. *(Corresponding Author: Guangwei Liu)*

Yu Li is with the School of Electrical Engineering, Shenyang University of Technology, Shenyang and 110870, China. (e-mail: 953525269@qq.com).

Guangwei Liu* is with the School of Electrical Engineering, Shenyang University of Technology, Shenyang and 110870, China. (e-mail: liu-gw@outlook.com and liugw@sut.edu.cn).

Wenping Cao is with the School of Engineering and Applied Science, Aston University, Birmingham and B4 7ET, UK. (e-mail: w.p.cao@aston.ac.uk).

Fengge Zhang is with the School of Electrical Engineering, Shenyang University of Technology, Shenyang and 110870, China. (e-mail: zhangfg@sut.edu.cn).

Digital Object Identifier 10.30941/CESTEMS.2022.00039

previous studies.

In this paper, study on high-speed machine silicon sheet electromagnetic characteristics, and calculation model of electromagnetic characteristics considering the coupling of magnetic field, stress and temperature is proposed. The accuracy of the two models was verified by a surface mount high speed permanent magnet synchronous motor. It provides valuable reference for permeability analysis and loss calculation of silicon steel sheet for high-speed machine, and also provides important reference for selection of silicon steel sheet for high-speed machine.

II. MAGNETIC PERMEABILITY CALCULATION MODE

The magnetic conductivity of silicon steel sheet is affected by various factors such as type, thickness, magnetic field, stress and temperature. According to the characteristics of its curve change [25]-[27], this paper fits its change of flux density according to gauss formula. K_{p1}-K_{p9} are determined by factors other than magnetic flux density, and the weight proportion of each factor is different. Therefore, the model can be expressed as follows.

$$\begin{cases} u = K_m\left(K_{p1}e^{-\left(\frac{B-K_{p2}}{K_{p3}}\right)^2} + K_{p4}e^{-\left(\frac{B-K_{p5}}{K_{p6}}\right)^2} + K_{p7}e^{-\left(\frac{B-K_{p8}}{K_{p9}}\right)^2}\right) \\ K_{pi} = r(\sigma)K_\sigma + r(t)K_t + r(f)K_f, i = 1 \sim 9 \\ r = \dfrac{\mathrm{Cov(X,Y)}}{\sqrt{D(\mathrm{X})}\sqrt{D(\mathrm{Y})}} \end{cases} \quad (1)$$

Where, the unit of permeability is mH/m, K_m is the magnetic field coefficient, which is affected by the magnetization mode and harmonics of the magnetic field, B is the magnetic flux density corresponding to the desired permeability, and r is the correlation coefficient, indicating the degree of correlation between X and Y. The closer the correlation coefficient is to 1, the greater X influence on Y. $r(\sigma)$ is the correlation coefficient between stress and permeability, similarly, $r(t)$ and $r(f)$ are the correlation coefficient between temperature and frequency and permeability, respectively. K_σ is the permeability coefficient only considered under stress, K_t is the permeability coefficient only considered under temperature, K_f is the permeability coefficient only considered under frequency, which are obtained by fitting magnetic permeability curves.

III. LOSS CALCULATION MODEL

A. Classical Loss Calculation Model

The alternation of the magnetic field causes the continuous movement and friction of the magnetic domain inside the silicon steel sheet, resulting in hysteresis loss. It also causes vortex effect outside the silicon steel sheet, resulting in eddy loss. The total loss generated is the iron loss of the motor.

From the microscopic point of view, the model divides iron loss into three parts according to the mechanism of iron loss, namely hysteresis loss P_h, eddy current loss P_c and additional loss P_e [28]. The expression of this model is

$$\begin{aligned} P &= P_h + P_c + P_e \\ &= k_h f B_m^\alpha + k_c f^2 B_m^2 + k_e f^{1.5} B \end{aligned} \quad (2)$$

Where k_h is the hysteresis loss coefficient, α is the Steinmetz coefficient. k_c is eddy current loss coefficient. k_e is additional loss coefficient. B_m is the magnitude of magnetic flux density. All the loss coefficients involved in this formula are obtained by fitting.

B. Loss Calculation Model Considering Magnetic Condition

In the actual operation of the motor, because the input excitation is not completely symmetric, the rotary magnetization is formed, which can be decomposed into two orthogonal magnetization which are perpendicular to each other and put into the formula. Due to its structural design and other reasons, there will be harmonics, resulting in the flux density waveform is not sinusoidal waveform, it can be decomposed into fundamental wave and harmonic wave, respectively into the formula, and then superimpose the calculation results. So, the calculation model is

$$\begin{aligned} P &= P_h + P_c + P_e \\ &= k_h f \sum_{k=1}^{\infty} k\left(B_{k\max}^\alpha + B_{k\min}^\alpha\right) + k_c f^2 \sum_{k=1}^{\infty} k^2\left(B_{\max}^2 + B_{\min}^2\right) \\ &\quad + k_e \frac{1}{T}\int_0^T \left(\left|\frac{dB_r(t)}{dt}\right|^2 + \left|\frac{dB_t(t)}{dt}\right|^2\right)^{\frac{3}{4}} dt \end{aligned} \quad (3)$$

Where, f is the frequency of 1 harmonic, and k is the harmonic order, B_{max} and B_{min} are the long-axis and short-axis magnetic flux density of the elliptic magnetic field, $B_r(t)$ and $B_t(t)$ are the radial and tangency magnetic flux density of the studied point at time t, and T is the period of the fundamental frequency.

C. Loss Calculation Model Considering Magnetic And Stress Condition

In addition to the factors of electromagnetic field, stress can also cause loss changes. The fundamental reason lies in the deformation of the silicon steel sheet caused by the action of stress, which leads to the change of the magnetic domain structure and movement mode inside the silicon steel sheet, thus changing the various loss coefficients. Therefore, when considering the coupling of magnetic field and stress field, each loss coefficient needs to be modified to obtain the loss calculation model under coupling.

$$\begin{aligned} P &= P_h + P_c + P_e \\ &= k_{h(\sigma)} f \sum_{k=1}^{\infty} k\left(B_{k\max}^\alpha + B_{k\min}^\alpha\right) + k_{c(\sigma)} f^2 \sum_{k=1}^{\infty} k^2\left(B_{\max}^2 + B_{\min}^2\right) \\ &\quad + k_{e(\sigma)} \frac{1}{T}\int_0^T \left(\left|\frac{dB_r(t)}{dt}\right|^2 + \left|\frac{dB_t(t)}{dt}\right|^2\right)^{\frac{3}{4}} dt \end{aligned} \quad (4)$$

Where, $k_{h(\sigma)}$, $k_{c(\sigma)}$ and $k_{e(\sigma)}$ are the hysteresis loss coefficient, the eddy current loss coefficient and the additional loss coefficient considering the influence of stress.

D. Loss calculation model considering magnetic, stress, and temperature condition

The change of temperature will also lead to the change of each loss coefficient, so when considering the coupling of

magnetic, stress, and temperature, the loss coefficient needs to be changed again. The improved loss calculation model is as follows:

$$\begin{aligned} P &= P_{\mathrm{h}} + P_{\mathrm{c}} + P_{\mathrm{e}} \\ &= (r_h(\sigma)k_{\mathrm{h}(\sigma)} + r_h(t)k_{\mathrm{h}(t)})\, f\sum_{k=1}^{\infty} k(B_{\mathrm{k\,max}}^{\alpha} + B_{\mathrm{k\,min}}^{\alpha}) \\ &+ (r_c(\sigma)k_{\mathrm{c}(\sigma)} + r_c(t)k_{\mathrm{c}(t)})f^2\sum_{k=1}^{\infty} k^2(B_{\max}^2 + B_{\min}^2) \\ &+ (r_e(\sigma)k_{\mathrm{e}(\sigma)} + r_e(t)k_{\mathrm{e}(t)})\frac{1}{T}\int_0^T \left(\left|\frac{dB_{\mathrm{r}}(t)}{dt}\right|^2 + \left|\frac{dB_{\mathrm{t}}(t)}{dt}\right|^2\right)^{\frac{3}{4}} dt \end{aligned} \tag{5}$$

Where, r is the correlation coefficient, and the corresponding relationship of each correlation coefficient is shown in Table I.

TABLE I
CORRELATION COEFFICIENT CORRESPONDENCE

Loss type	Stress	Temperature
hysteresis loss	$r_{\mathrm{h}}(\sigma)$	$r_{\mathrm{h}}(t)$
eddy current loss	$r_{\mathrm{c}}(\sigma)$	$r_{\mathrm{c}}(t)$
additional loss	$r_{\mathrm{e}}(\sigma)$	$r_{\mathrm{e}}(t)$

IV. FEM ANALYSIS OF SMHSPMSM

A. Basic Parameters And Structure of the Motor

The basic parameters of the motor are shown in Table II, and the structure model is shown in Fig. 1.

TABLE II
BASIC PARAMETERS OF THE MOTOR

Parameter	Numerical value
Rated power /kW	160
Rated voltage /V	380
Rated speed /rpm	17000
Poles	4
Slots	36

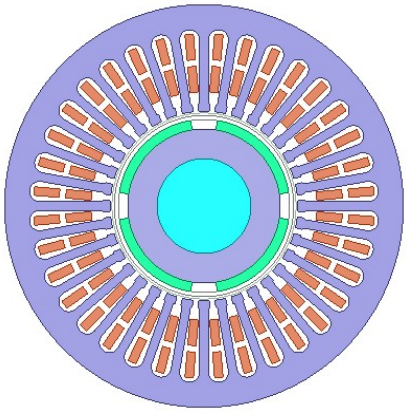

Fig. 1. Motor structure model.

As the silicon steel sheet is often used as the stator core, the stator silicon steel sheet is mainly located in the area when the motor field analysis.

B. Magnetic Field Analysis of the Motor

In order to better analyze the magnetic field of the motor, any set of slots is taken from the completely symmetrical slots structure. The finite element method is used to select 9 feature points on the stator. The points are shown in the Fig. 2.

During the operation of the motor, its magnetization method

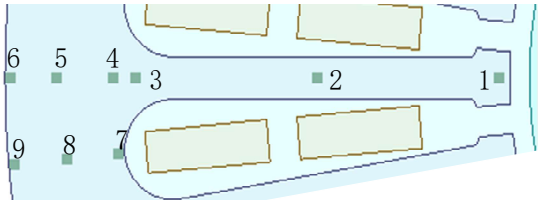

Fig. 2. Stator feature point distribution.

is different from that when the silicon steel sheet is static. Not only there is an alternating magnetic field, but also a rotating magnetic field. In this paper, the rotating magnetic field is decom-posed into two mutually orthogonal alternating magnetic fields for analysis.

Taking feature point 3 as an example, the schematic diagram of rotating magnetization and decomposition is shown in the Fig. 3.

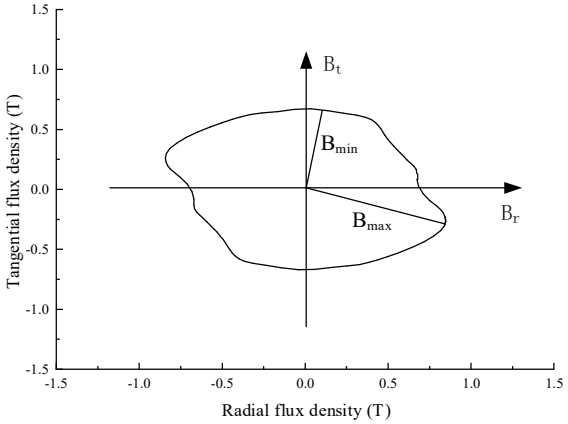

Fig. 3. Feature point 3 rotating magnetization and decomposition diagram.

Though Fig. 3 that its shape is not a standard ellipse, and the reason is that it contains the influence of harmonics. Also take feature point 3 as an example to perform harmonic analysis, and the decomposed magnetization locus results are shown in Fig. 4.

Therefore, when studying the electromagnetic properties of silicon steel sheet, the influence of magnetization mode and harmonics cannot be ignored.

C. Stress Field Analysis of the Motor

Inside the motor, the stator core is affected by the combined effects of electromagnetic force and the assembly stress generated by the casing.

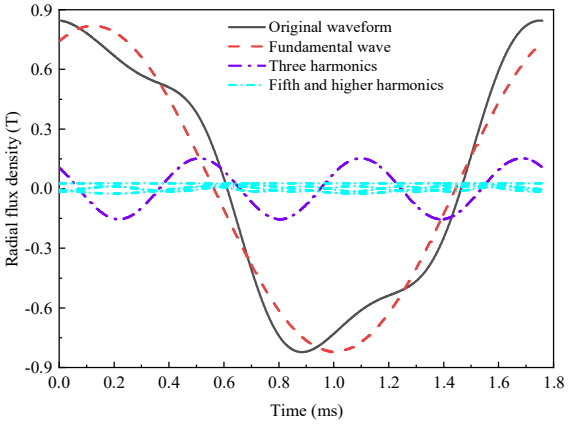

(a)

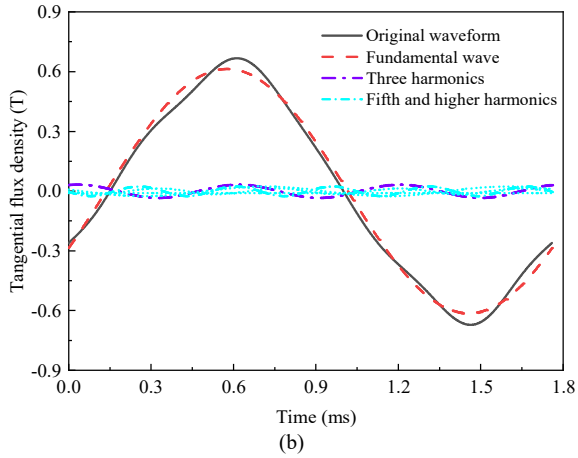

(b)

Fig. 4. Feature point 3 Fourier decomposition diagram; (a) Fourier decomposition of radial flux density and (b) Tangential flux density Fourier decomposition.

It is formula of radial electromagnetic force generated by air gap magnetic field of electric machine.

$$P = B^2(\theta,t) / 2\mu_0 \tag{6}$$

Where $B^2(\theta,t)$ is the air gap magnetic density that changes in space and time, μ_0 is air permeability.

From this, get the variation curve of electromagnetic force between stator and rotor, it is shown in Fig. 5. It was observed that the effective value is 0.1225MPa and the maximum value is 0.1647MPa.

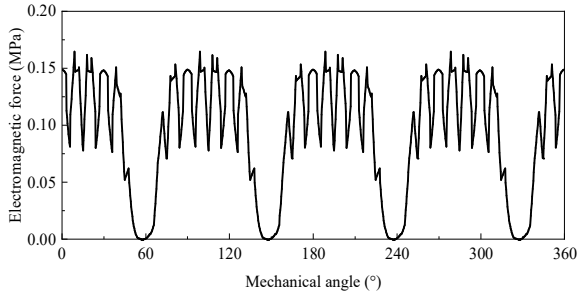

Fig. 5. Electromagnetic force variation curve.

Interference assembly of the frame and stator produces radial compressive stress on the stator. And the interference is set as 0.2 mm. The FEM simulation result is shown in Fig 6.

According to Fig. 6, the maximum stress occurs at the bottom of the stator slot and the minimum stress occurs at the stator yoke, with the values of 121.09MPa and 9.5514MPa.

It was observed that the electromagnetic force is far less than the extrusion stress of the housing, and can be ignored.

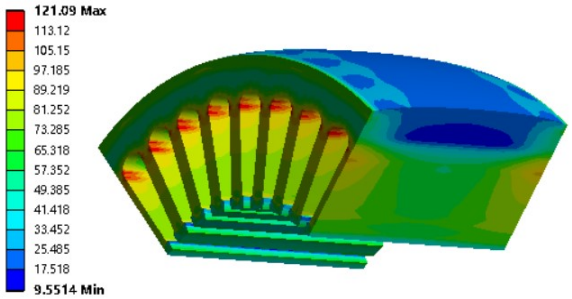

Fig. 6. Stress distribution of stator.

D. Temperature Field Analysis of the Motor

When the motor is in natural heat dissipation, the simulation conditions of the static temperature field are as follows:

(1) Iron loss of stator, winding loss, and eddy current loss of rotor are set as heat sources.

(2) The axial symmetry planes on both sides of the model were set as adiabatic.

(3) The head face of stator and rotor, winding head face, housing and air gap are given different heat dissipation coefficients.

After FEM analysis, its temperature distribution is shown in Fig. 7.

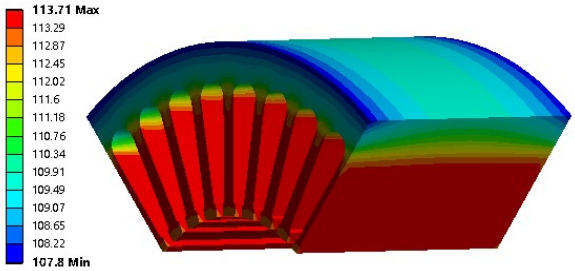

Fig. 7. Temperature distribution of stator.

It was observed that the maximum temperature occurs at the stator teeth and the minimum temperature occurs at the stator yoke, with the values of 113.71℃ and 107.8℃.

E. Field Coupling Analysis of the Motor

The magnetic, stress and temperature are iteratively coupled through the coupling process shown in Fig. 8. The temperature distribution, stress distribution and simulation value of electromagnetic characteristics of silicon steel sheet can be obtained when the three are coupled to a stable state.

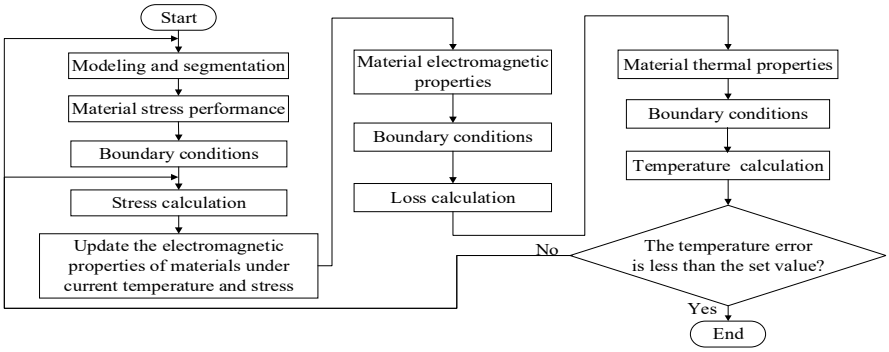

Fig. 8. Magnetic, stress, and temperature coupling flow chart.

V. MEASUREMENT AND ANALYSIS OF ELECTROMAGNETIC CHARACTERISTICS

A. Measuring Device and Measuring Method

In this paper, the model of silicon steel sheet B20AT1500 is measured by a single silicon steel sheet electromagnetic performance measuring instrument. Measuring device and schematic diagram of measuring are shown in Fig. 9. Parameter setting and measurement conditions in the experiment are shown in Table III.

Fig. 9 (a) show that the silicon steel sheet and the yoke form a connected magnetic circuit. Excitation is input at one end of the yoke, and magnetic field intensity and flux density are induced at the other end. The device shown in Fig. 9 (b) can uniformly apply compressive stress on the silicon steel sheet, and the stress direction is perpendicular to the rolling direction, which is consistent with the stress direction of the stator. The device shown in Fig. 9 (c) can be applied at any temperature. The loss and permeability data can be obtained through the measurement device and data processing platform.

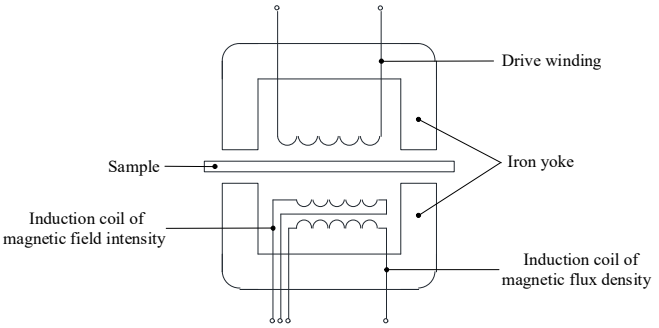

(a)

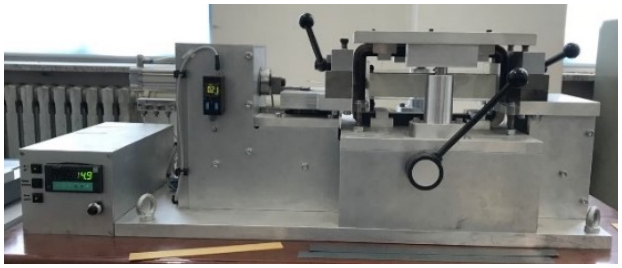

(b)

(c)

Fig. 9. Electromagnetic characteristic measuring instrument; (a) Schematic diagram of a single silicon steel sheet electromagnetic performance measuring instrument, (b) Stress effect measuring instrument, (c) Temperature effect measuring instrument.

TABLE III
PARAMETER SETTING AND MEASURING CONDITIONS

Parameters and Conditions	Options and Values
Supply voltage /V	220
Input waveform	sine wave
Frequency range of measurement /Hz	50-1000
Flux density range of measurement /T	0.1-1.8
Stress range of measurement /MPa	0-100
Temperature range of measurement /℃	20-200

B. Analysis of Magnetic Permeability

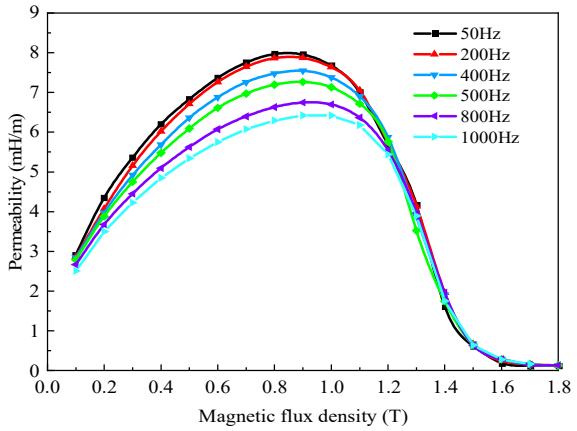

(a)

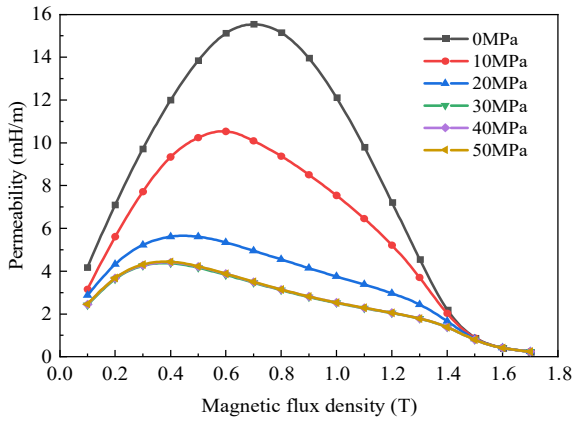

(b)

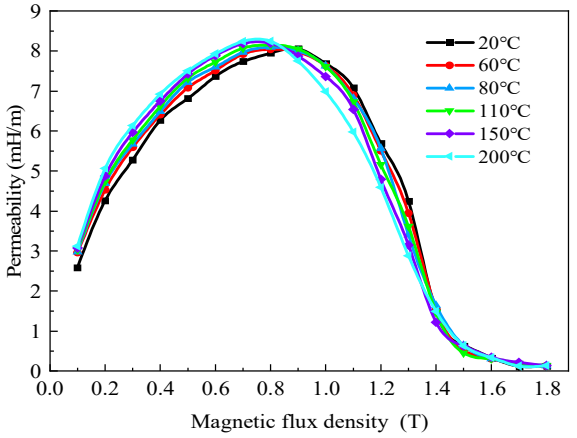

(c)

Fig. 10. Permeability curves of various factors; (a) Permeability curves of various frequencies, (b) Permeability curves of various stress, and (c) Permeability curves of various temperature.

Fig. 10 (a) to (c) are the change curves of the magnetic permeability of silicon steel sheets in the influence of magnetic, temperature, and stress separately.

Fig. 10 (a) shows the magnetic permeability of silicon steel sheets of different frequencies when T=20℃ and P=0MPa. The conclusion is shown as magnetic permeability decreases with the increase of frequency, and the correlation coefficient is 0.1937.

Fig. 10 (b) shows the magnetic permeability of silicon steel sheets of different stress when f=50Hz and T=20℃. Obtain the following conclusion: The permeability decreases rapidly with the increase of compressive stress and remains from 30MPa, and the correlation coefficient is 0.7144.

Fig. 10 (c) shows the permeability of the silicon steel sheet at different temperatures when f=50Hz and P=0MPa. The conclusion is before the saturation point, the permeability rises faster with the increase of temperature. After the saturation point, it falls slower. And the correlation coefficient is 0.0234.

When magnetic is coupled with temperature and stress respectively, the influence of various factors on permeability changes, as shown in the Fig. 11.

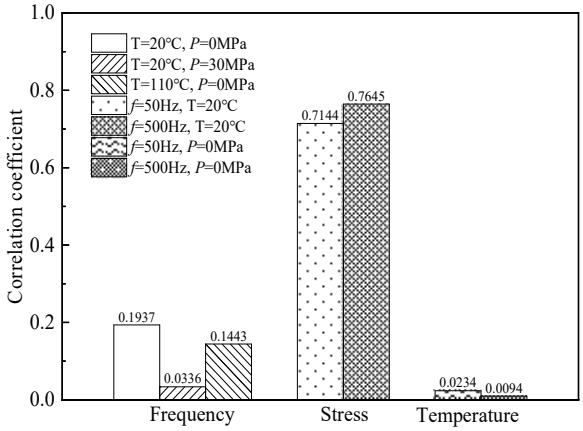

Fig. 11. Permeability change at different factors.

Here are the results we got from Fig. 11. (1)The influence of frequency on permeability is affected by compressive stress and temperature, and compressive stress accounts for a large proportion. (2)The influence of compressive stress on permeability is not affected by the magnetic field. (3) The influence of temperature on permeability is slightly affected by frequency.

It was observed that the conclusion is the influence on permeability of com-pressive stress is far more than the influence of frequency, temperature barely has influence on permeability, Whether each factor is considered separately or coupled.

C. *Analysis of Loss*

Fig. 12 (a) to (c) are the change curve of silicon steel sheet loss in the influence of magnetic, stress, and temperature separately.

Fig. 12 (a) shows the curve of silicon steel sheet loss at different frequencies when T=20℃ and P=0MPa. The loss increases with increasing frequency and magnetic flux density, especially at high frequency and great flux densities, the loss increases faster.

Fig. 12 (b) shows the curve of silicon steel sheet loss at different stress when f=50Hz and T=20℃. The loss increases with the increase of stress, and remains from 30MPa.

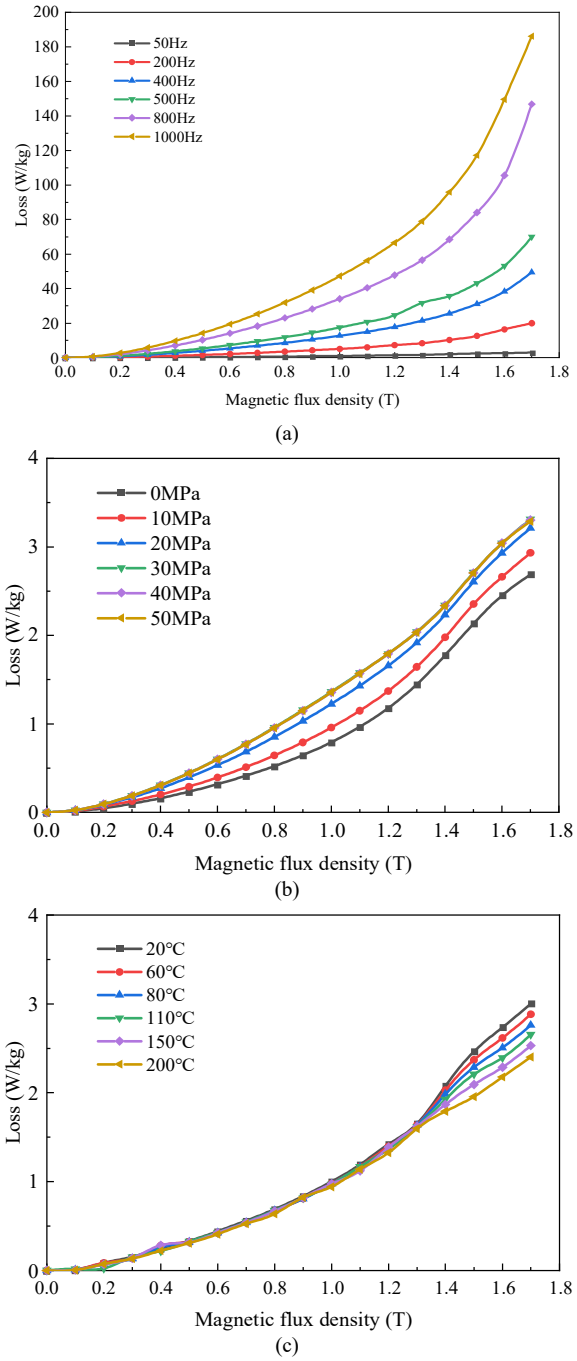

Fig. 12. Loss curves of various factors; (a) Loss curves of various frequencies, (b) Loss curves of various stress, and (c) Loss curves of various temperature.

Fig. 12 (c) shows the curve of silicon steel sheet loss at different temperatures when f=50Hz and P=0MPa. The loss decreases with the increase of temperature, and the proportion of loss reduction increase with the increase of temperature.

When magnetic is coupled with stress and temperature respectively, the influence of various factors on loss changes, as shown in the Fig. 13.

Here are the conclusions. (1) The effect of frequency on loss is weakened by compressive stress and enhanced by temperat-

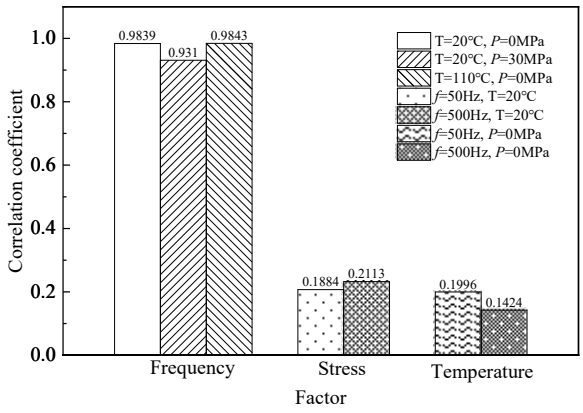

Fig. 13. Loss change at different factors.

ure. (2) The increase in frequency weakens the in-fluence of temperature on loss, and enhances the influence of compressive stress on loss.

According to the above study which shown that (1) Frequency has the greatest influence on loss, temperature is the second, and stress is the least when consider these factors in individually. (2) The influence of compressive stress on loss surpasses temperature when coupling of three factors.

VI. Calculation and Verification of Electromagnetic Characteristics

A. Calculation and Verification of Permeability

In this section, the permeability calculation model is applied into the SMHSPMSM for calculation, and the calculation results of each feature point are compared with the simulation results to verify the accuracy of the model.

Because the permeability calculation model is affected by magnetic, stress, and temperature, the value of each factor directly affects the accuracy of the calculation results. The frequency is known and it's not changing, we don't have to evaluate it. Instead of using a global average for stress and temperature, it is divided into four regions, with different averages for each region. The partitioning diagram is shown in Fig.14.

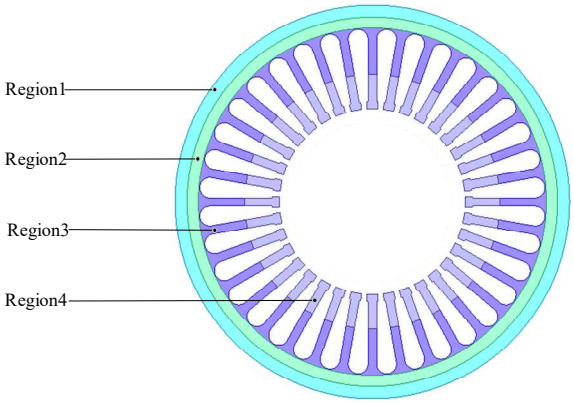

Fig. 14. Partition diagram of stator.

The average stress and average temperature of each region were obtained of FEM, and the correlation coefficients of each factor were calculated, as shown in Table IV. As can be seen that the variation range of $r(\sigma)$ is large, while that of $r(t)$ and $r(f)$ is small, and its variation trend is consistent with the conclusion obtained in the experiment.

TABLE IV
FACTORS AND CORRELATION COEFFICIENT OF DIFFERENT REGION

Region	Factor	$r(\sigma)$	$r(t)$	$r(f)$
1	f=567Hz, P=13MPa, T=108℃	0.3220	0.0067	0.1017
2	f=567Hz, P=28MPa, T=109℃	0.6388	0.0069	0.0426
3	f=567Hz, P=90MPa, T=111℃	0.7645	0.0072	0.0326
4	f=567Hz, P=55MPa, T=113℃	0.7645	0.0076	0.0329

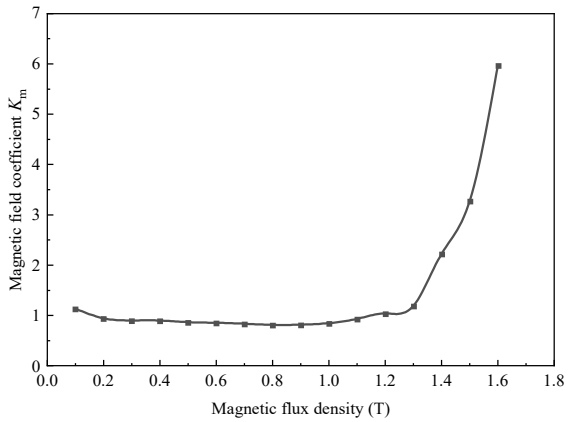

Fig. 15. Magnetic field coefficient curve.

It is affected by the magnetization mode and harmonics in the magnetic field. When the flux density is small, K_m changes little and fluctuates around 1. When the flux density is large, K_m increases linearly. The relationship between K_m and magnetic flux density is shown in the Fig. 15.

The calculated values of each feature point are obtained by apply the above coefficients to calculate the permeability. The above experiment shows that the influence of stress on permeability is greater than that of temperature. Therefore, In the simulation calculation of this paper, the B-H curve is only composed of experimental data of different stresses. Expression (8) is brought into the field calculator for simulated, and the simulation values of each feature point are obtained.

$$\mu_c = \sqrt{\left(\frac{B_r}{H_r}\right)^2 + \left(\frac{B_t}{H_t}\right)^2} \tag{7}$$

Where B_r and B_t are radial and tangential flux densities respectively, H_r and H_t are radial and tangential magnetic field intensity.

The Table V shows the comparison between calculated and simulated values. As can be seen from the table that the maximum error is 4.7%, the minimum error is 0.1%, and the average error between the calculated value and the simulated value is 3.9%, which indicates that the calculation model has high accuracy.

TABLE V
THE PERMEABILITY OF EACH FEATURE POINT

Feature point	Simulation value μ_s (mH/m)	Calculated value μ_c (mH/m)	Error (%)
1	3.582	3.414	4.7
2	3.251	3.244	0.2
3	3.879	3.863	0.4
4	5.172	5.146	0.5
5	5.081	5.025	1.1
6	5.120	5.043	1.5
7	4.838	4.596	5.0
8	5.240	5.235	0.1
9	7.327	7.173	2.1

B. Calculation and Verification of Loss

In the calculation of loss, additional loss accounts for a relatively small proportion, so it is ignored in the calculation of loss in this section. Due to different calculation models and different factors, the loss coefficient in each model is different. When the frequency is 567Hz, the loss curves obtained in the experiment are fitted to obtain the loss coefficients of different stresses and temperatures, as shown in Fig. 16 and Fig. 17.

It can be seen from Fig. 16 that when the compressive stress is between 0 and 30 MPa, the hysteresis loss coefficient increases linearly, When the stress is greater than 30 MPa, it is basically steady. and the eddy current loss coefficient only fluctuates in a small amplitude around 0.27.

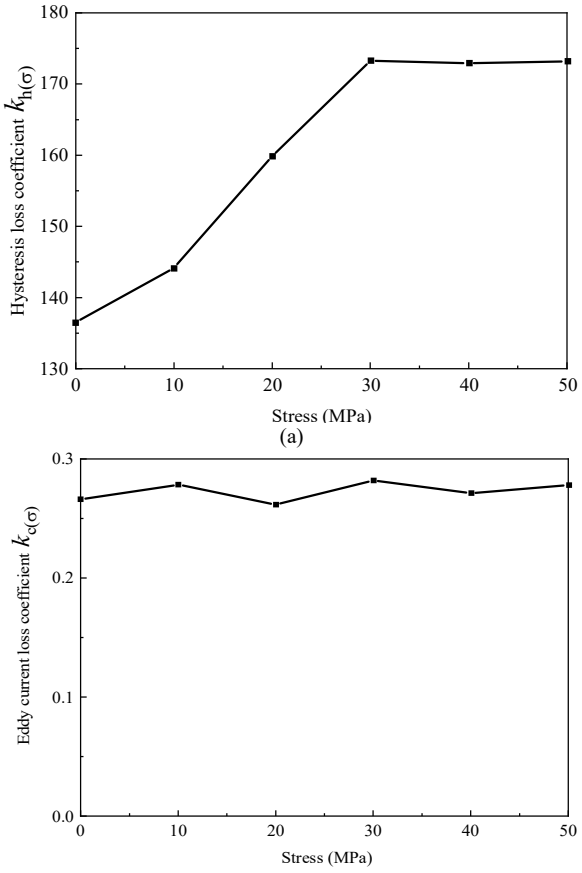

Fig. 16. Loss coefficients of various stress; (a) Hysteresis loss coefficient and (b) Eddy current loss coefficient.

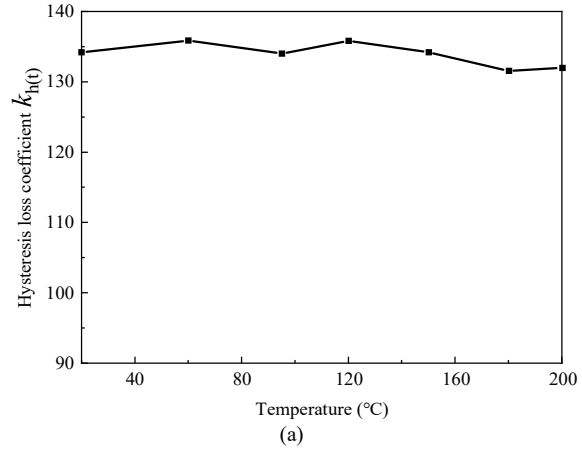

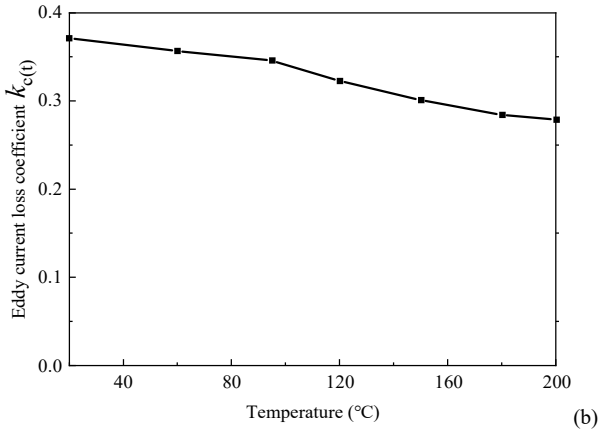

Fig. 17. Loss coefficients of various temperature; (a) Hysteresis loss coefficient and (b) Eddy current loss coefficient.

Through Fig. 17, the hysteresis loss coefficient only fluctuates slightly around 135, while the eddy current loss decreases linearly with the increase of temperature.

Therefore, the hysteresis loss coefficient has a stronger correlation with stress and a weaker correlation with temperature. The eddy current loss coefficient is the opposite.

Average stress and average temperature of each region were obtained through coupling simulation, and correlation coefficients each region were calculated, as shown in Table VI. It was observed that $r_h(\sigma)$ is much larger than $r_h(t)$, and $r_c(t)$ is much larger than $r_c(\sigma)$, which is consistent with the experimental conclusion.

TABLE VI
FACTORS AND CORRELATION COEFFICIENT OF DIFFERENT REGION.

Region	Factor	$r_h(\sigma)$	$r_h(t)$	$r_c(\sigma)$	$r_c(t)$
1	*f*=567Hz *P*=13MPa T=108℃	0.9805	0.0036	0.2627	0.9692
2	*f*=567Hz *P*=28MPa T=109℃	0.9914	0.0036	0.3053	0.9782
3	*f*=567Hz *P*=90MPa T=111℃	0.9673	0.0034	0.2583	0.9840
4	*f*=567Hz *P*=55MPa T=113℃	0.9314	0.0032	0.3027	0.9843

The calculation results of each model can be obtained by applying the above conditions. And during the simulation calculation, the loss data measured by the experiment of various factors are first imported into the material library, then the loss is simulated by using the finite element software's own solution model. The calculation results and simulation results are shown in the Table VII .

TABLE VII
LOSS CALCULATION VALUES AND SIMULATION VALUE.

Loss calculation model	Value / W
Classical loss calculation model	1005.112
Considering magnetic condition	1312.040
Considering magnetic and stress condition	1401.541
Considering magnetic, stress, and temperature condition	1379.106
Simulation value	1341.068

As can be seen from the Table VII, the calculated loss value increases gradually with the increase of the factors considered.

Compared with the classical loss calculation model, the loss value obtained by each model increases by 30.54%, 39.44% and 37.84% respectively. This shows that the effect of magnetic and stress results in the increase of loss, while the effect of temperature reduces the loss. Which is consistent with the conclusion of the silicon steel sheet loss experiment. Because the rotation magnetization and harmonics of every point on the silicon steel sheet cannot be processed in the simulation, the loss value obtained is lower than the calculated value considering magnetic, stress, and temperature condition. Then, the difference was 3.3%.

VII. Conclusions

In this paper, the field of the motor at work is analyzed to obtain the distribution characteristics of magnetic field, stress field and temperature field. Considering the influence of multiple factors, the electromagnetic characteristics of the silicon steel sheet for the motor are studied and the conclusions are as follows:

(1) Magnetic, stress, and temperature will lead to the decline of magnetic conductivity of silicon steel sheet. And stress has the greatest impact on magnetic permeability, the second is magnetic, and the influence of temperature is smallest.

(2) The loss of the silicon steel sheet increases due to the action of magnetic field and stress, and decreases due to the action of temperature. Frequency has the greatest influence on loss, temperature is the second, and stress is the least when consider these factors in individually. The influence of compressive stress on loss surpasses temperature when coupling of three factors.

(3) The permeability coefficient is affected by many factors. The stress correlation coefficient is the largest, with an average of 0.7, and the frequency correlation coefficient is 0.04.

(4) The hysteresis loss coefficients are mainly affected by stress, and their correlation coefficients are all greater than 0.9. The eddy current loss coefficients are mainly affected by temperature, and their correlation coefficients are all greater than 0.9.

(5) The calculation models of permeability and loss are verified by simulation, and the errors between the calculated values and simulation values are less than 5%.

References

[1] F. F. Zhang, G. H. Du, T. Y. Wang, F. X. Wang, W. P. Cao and J. L. Kirtley. “Electromagnetic design and loss calculations of a 1.12-MW high-speed permanent-magnet motor for compressor applications”. *IEEE Transactions on Energy Conversion*. vol. 31, no. 1, pp. 132-140, Mar. 2016.

[2] F. R. Ismagilov, N. Uzhegov, V. E. Vavilov, V. I. Bekuzin and V. V. Ayguzina. “Multidisciplinary design of ultra-high-speed electrical machines”. *IEEE Transactions on Energy Conversion*. vol. 33, no. 3, pp. 1203-1212, Sept. 2018.

[3] N. Fernando, P. Arumugam, and C. Gerada. “Design of a stator for a high-speed turbo-generator with fixed permanent magnet rotor radius and volt–ampere constraints”. *IEEE Trans on Energy Conversion*. vol. 33, no. 3, pp. 1311–1320, Sept. 2018.

[4] N. Bernard, R. Missoum and L. Dang, N. Bekka, H. Ben Ahmed and M. E. Zaïm.. “Design methodology for high-speed permanent magnet synchronous machines”. *IEEE Trans on Energy Conversion*. vol. 31, no. 2, pp. 477–485, Jun. 2016.

[5] G. W. Liu, M. Y. Liu, Y. Zhang, H. J. Wang and C. Gerada. (). “High-Speed permanent magnet synchronous motor iron loss calculation method considering multiphysics factors”. *IEEE Transactions on Industrial Electronics*, vol. 67, no, 7, pp. 5360-5368, Jul. 2020.

[6] D. P. Wang, T. Ma. “Loss and temperature field analysis of permanent magnet brushless DC high speed motor with two rotor structures”, *Journal of Electrical Engineering*, vol. 13, no. 8, pp. 12-17, Aug. 2018.

[7] W. M. Tong, S. H. Dai, S. N. Wu, and R. Y. Tang. “Performance comparison between an amorphous metal PMSM and a silicon steel PMSM”, *IEEE Transactions on Magnetics*, vol. 55， no. 6, pp. 1-5, Jun. 2019.

[8] J. Ou, Y. Z. Liu and M. Doppelbauer. Comparison study of a surface-mounted PM rotor and an interior PM rotor made from amorphous metal of high-speed motors. *IEEE Transactions on Industrial Electronics*. vol. 68, no. 10, pp. 9148-9159, Oct. 2021.

[9] V. Maurel, F. Ossart and R. Billardon. “Residual stresses in punched laminations, phenomenological analysis and influence on the magnetic behavior of electrical steels”. *Journal of Applied Physics.* vol. 93, no. 10, pp. 7106-7108, May, 2003.

[10] H. Naumoski, B. Riedmüller, A. Minkow and U. Herr. “Investigation of the influence of different cutting procedures on the global and local magnetic properties of non-oriented electrical steel”. *Journal of Magnetism & Magnetic Materials*. vol. 39, no. 2, pp. 126-133, May, 2015.

[11] Y. Rong, Q. Y. Kong, W. D. Qi, S. H. Liu, C. Li and Z. K. Luo. “Studies on the Building Factor of Transformers Based on laminated Core Models”. In *Proc. of 2019 22nd International Conference on Electrical Machines and Systems (ICEMS)*. pp. 1-5, Aug. 2019.

[12] Paolinelli S C, Cunha M A D. “Effect of stress relief annealing temperature and atmosphere on the magnetic properties of silicon steel”. *Journal of Magnetism and Magnetic Materials*, vol. 304, no. 2, pp. e599-e601, Feb. 2006.

[13] C. G. Zhang, X. X. Yan, Y. J. Li and Q. X. Yang. “Vector magnetic properties measurement of silicon steel under biased magnetic excitation along laminated direction”. *IEEE Transactions on Magnetics*. vol. 55, no. 2, pp. 1-4, Feb. 2019.

[14] R. Homma and Y. Ohsugi. “Improved post 1-D analysis using distribution of differential magnetic permeability”. *IEEE Transactions on Magnetics*. vol. 57, no. 6, pp. 1-4, Jun. 2021.

[15] C. G. Zhang, Y. J. Li, J. S. Li, Q. X. Yang and J. G. Zhu. “Measurement of three-dimensional magnetic properties with feedback control and harmonic compensation”. *IEEE Transactions on Industrial Electronics*. vol. 64, no. 3, pp. 2476-2485, Mar. 2017.

[16] R. Y. Chen, C. G. Zhang, Y. J. Li, Q. X. Yang and L. X. Wang. “An improved method for measuring the magnetic properties of silicon steel with double sheets at high frequency”. *IEEE Transactions on Magnetics*. vol. 55, no. 2, pp. 1-4, Feb. 2019.

[17] Y. Dou, Y. J. Li, C. G. Zhang, S. C. Yue and J. G. Zhu. “Effects of uniaxial stress along different directions on alternating magnetic properties of silicon steel sheets”. *IEEE Transactions on Magnetics*. vol. 56, no. 3, pp. 1-4, Mar. 2020.

[18] D. Miyagi, D. Otome, M. Nakano, and N. Takahashi. “Measurement of magnetic properties of Nonoriented electrical steel sheet at liquid nitrogen temperature using single sheet tester”. *IEEE Transactions on Magnetics*. vol. 46, no. 2, pp. 314-317, Feb. 2010.

[19] S. Takajo, T. Hiratani, T. Okubo, and Y. Oda. “Effect of silicon content on iron loss and magnetic domain structure of grain-oriented electrical steel sheet”. *IEEE Transactions on Magnetics.* vol. 54, no. 1, pp. 1-6, Jan. 2018.

[20] T. Yoshioka, T. Tsuge, Y. Takahashi, and K. Fujiwara. “Iron loss estimation method for silicon steel sheet taking account of DC-biased conditions”. *IEEE Transactions on Magnetics*. vol. 55, no. 6, pp. 1-4, Jun. 2019.

[21] X. J. Zhao, H. W. Xu, Z. G. Cheng, Z. B. Du, L. Zhou and D. W. Yuan. “A simulation method for dynamic hysteresis and loss characteristics of GO silicon steel sheet under non-sinusoidal excitation”. *IEEE Transactions on Applied Superconductivity*. vol. 31, no. 8, pp. 1-4, Nov. 2021.

[22] Oda Y, Hiratani T, Kasai S, Tomoyukiokubo, Senda, K, and Chiba, A. “Effect of compressive stress on iron loss of gradient Si steel sheet”. *Electronics and Communications in Japan*. vol. 99, no. 12, pp. 74-83, Dec. 2016

[23] M. Lobue, C. Sasso, and V. Basso. “Power losses and magnetization process in Fe-Si non-oriented steels under tensile and compressive stress”. *J. Magn. Magn. Mater*, vol. 215, no. 3, pp. 124-126, Jun. 2000.

[24] N. Takahashi, M. Morishita, D. Miyagi, and M. Nakano. “Comparison of magnetic properties of magnetic materials at high temperature”. IEEE Transactions on Magnetics, vol. 47, no. 10, pp. 4352-4355, Oct. 2011

[25] D. Miyagi, K. Miki, M. Nakano, and N. Takahashi. “Influence of compressive stress on magnetic properties of laminated electrical steel sheets”. *IEEE Transactions on Magnetics*, vol. 46, no. 2, pp. 318-321, Mar, 2010.

[26] K. Yamazaki and H Takeuchi. “Impact of mechanical stress on characteristics of interior permanent magnet synchronous motors”. *IEEE Transactions on Industry Applications*, vol. 53, no. 2, pp. 963-970, Mar, 2017 .

[27] W. M. Tong, S. Q. Li, R. L. Sun, L. Sun, and R. Y. Tang. “Modified core loss calculation for high-speed PMSMs with amorphous metal stator cores”. *IEEE Transactions on Energy Conversion*, vol. 36, no. 1, pp. 560-569, Mar, 2021.

[28] X. T. Zhang, P. R. Fu, Y. G. Ma, C. M. Zhang, L. Y. Li. “No-Load iron loss model for a fractional-slot surface-mounted permanent magnet motor based on magnetic field analytical calculation”. *Chinese Journal of Electrical Engineering*. vol. 4, no. 4, pp. 71-79, Dec. 2018.

Yu Li received the B.S degree in electrical engineering from Heilongjiang Bayi Agricultural University, Daqing, China, in 2018. He is currently pursuing the M.S. degree in electrical engineering from the Shenyang University of Technology. His main fields of interest are modeling and analysis of silicon steel sheet electromagnetic characteristics.

Guangwei Liu (M'17) received the B.E.E., M.S., and Ph.D. degrees in electrical engineering from the Shenyang University of Technology, Shenyang, China, in 2005, 2008, and 2015, respectively, He is currently a Professor of Electrical Machines with the School of Electrical Engineering, Shenyang University of Technology, Shenyang, China. His major research interests and activities are in the areas of permanent magnet electrical machines and its drive system.

Wenping Cao (M'05–SM'11) received the B.Eng. degree in electrical engineering from Beijing Jiaotong University, Beijing, China, in 1991, and the Ph.D. degree in electrical machines and drives from the University of Nottingham, Nottingham, U.K., in 2004. He is currently a Chair Professor of Electrical Power Engineering and the Head of the Power Electronics, Machines, and Power System Group, Aston University, Birmingham, U.K.

Fengge Zhang (M'17) received the B.E.E., M.S., and Ph.D. degrees from the Shenyang University of Technology, Shenyang, China, in 1984, 1990, and 2000, respectively, all in electrical engineering. Since 1984, he has been with the School of Electrical Engineering, Shenyang University of Technology, where he is currently a Professor. His research and teaching interests include electromagnetic theory, dynamic simulation, magnetic field analysis, optimized design, computer control technology of electrical machines, and wind power generating systems.